Fizika Nizkikh Temperatur, 2000, v. 26, Nos. 9/10, p. 947–962

Physical aspects of matrix isolation technique: FTIR studies on CO and CO_2 in O_2 and N_2 matrices

Maksym Minenko, Martin Vetter, Alexander P. Brodyanski, and Hans J. Jodl

Fachbereich Physik, Universität Kaiserslautern, Erwin Schrödinger Str., 67663 Kaiserslautern, Germany
E-mail: jodl@physik.uni.-kl.de

Received April 26, 2000

The matrix isolation technique is traditionally used to investigate the properties of the matrix-isolated species themselves or to solve some special questions of the theory of defects in solid. We showed here that the optical spectroscopy of really matrix-isolated molecules can be successfully used to investigate the host crystal qualities too. We demonstrated the capacity of modern FTIR spectroscopy to study the properties of cryocrystals such as phase transitions, solubility boundaries, orientational order parameter, etc. by monitoring the behavior of the IR-active molecules, which are present in matrices under investigation as a natural contamination (40 ppb). Due to the excellent optical quality of our crystal samples, we were able to determine a part of the binary phase diagram CO-O_2 (at CO concentrations less than 1 ppm) as well as to investigate the kinetics of phase transitions. Furthermore, we successfully used the spectroscopy of the matrix-isolated molecules to proof that the α–β phase transition of the matrix crystal (O_2) is of first order.

PACS: 33.20.Ea

1. Introduction

The matrix isolation (MI) technique is used in general to investigate properties of the isolated molecules (or small groups of them) such as their shape, their spectrum, the relaxation of molecule excitations, etc. as well as their chemical and physical behavior. Recently [1], we have shown that the matrix isolation technique can be also successfully used to render some principal important information on the properties of the host crystal, where these molecules were dissolved (CO, CO_2 in N_2 matrix). The principal prerequisite to employ the MI technique for this special purpose is to work with a *real* MI case to avoid any segregation processes, cluster formation and to neglect any interaction between dissolved impurities. The basic physical idea of our approach is relatively simple: the spectroscopic characteristics of the internal vibrations of a well isolated molecule (frequency, bandwidth) are unambiguously determined only by the properties of this molecule itself and a crystal field of the host crystal in which this molecule is embedded. Changes in the crystal field varying external conditions (such as temperature, pressure) cause corresponding changes in spectroscopic characteristics of the MI molecule. Therefore, by monitoring the behavior of this MI molecule carefully, we can probe the host crystal qualities such as phase transitions, intermolecular distance, order parameter, dynamics and relaxation processes, etc. Moreover, starting from a *real* MI case it is possible to investigate the low concentration part of the phase diagram of binary systems correctly. Our previous results [1] change traditional opinions about MI case such as the solubility limit in cryocrystals; we have shown that the thermodynamic equilibrium solubility limit for CO_2 molecules in solid nitrogen is lying at molar concentrations about 10^{-7}–10^{-6}.

FTIR spectroscopy is a substantially more sensitive tool in comparison with Raman scattering to investigate small impurity concentrations. Therefore, it is meaningful to employ IR-active MI molecules to probe indirectly of host crystal qualities of spectroscopically inactive matrices (rare gas solids, etc.). In Fig. 1, we present the internal vibration spectrum of CO molecules, MI in solid oxygen. Our oxygen gas used (purity 99.998%) contains these CO molecules as a residual contamination. Analyzing the integrated intensity of this peak in combination with known absorption coefficient of CO, we determined the CO concentration in solid oxygen to be $4 \cdot 10^{-8}$.

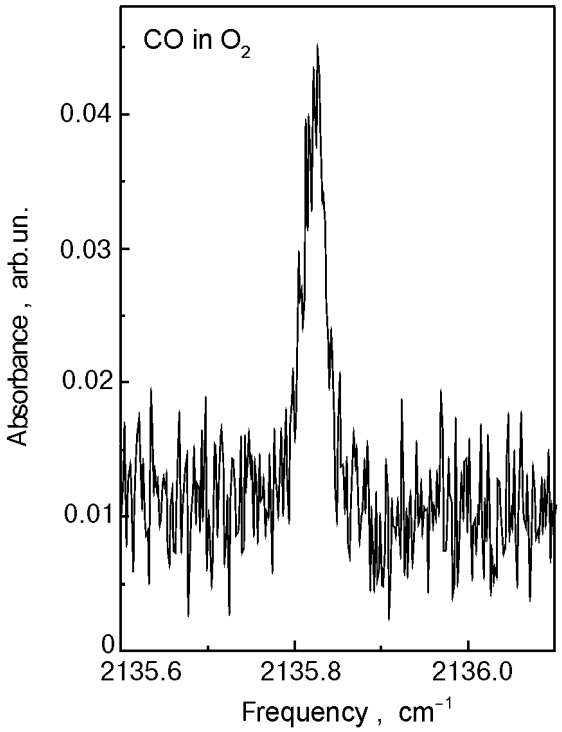

Fig. 1. Mid IR spectrum of the internal vibration of the CO molecules matrix isolated in α-oxygen (T = 11 K, spectral resolution 0.003 cm^{-1}). The CO molecules are present in our oxygen (99.998%) as a residual contamination (CO/O_2 ratio $\sim 4 \cdot 10^{-8}$)

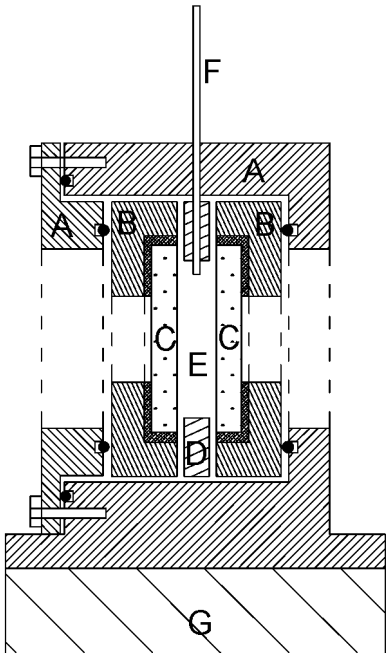

Fig. 2. The sample cell specially designed for IR-spectroscopic investigations of cryocrystals and their mixtures at zero pressure.

Our aim is to study the *real* matrix isolated case and to probe solid-state aspects of the matrix. We had chosen CO_2 and CO molecules matrix isolated in solid nitrogen and oxygen as an example. Our paper is structured as follows: in Sec. 2, we briefly describe our experimental procedure (method, crystal growth, determination of impurity concentration, etc.). Experimental results are presented together with the discussion in one section. We will analyze first the phase transitions in the host crystals. Second, we will interpret the behavior of mode frequency to gain information on host crystal qualities; third, we will study the low concentration part of the phase diagrams (CO_2 in nitrogen and oxygen as well as CO in oxygen); fourth, we will discuss mode relaxation processes of impurities in these selected cryocrystals.

2. Experimental procedure

We investigated the CO_2 and CO molecules dissolved in condensed phases of nitrogen and oxygen at equilibrium vapor pressure by FTIR spectroscopy in the temperature range from 10 to 90 K. The spectra of the impurity fundamentals were recorded in the mid infrared spectral region by a Fourier spectrometer (Bruker IFS 120 HR). Two sets of light sources and beam splitters were used: a glowbar source and a KBr beam splitter (spectral range 800–5000 cm^{-1}) as well as a tungsten lamp and a CaF_2 beam splitter (spectral range 1900–11000 cm^{-1}). The diameter of the diaphragm was 1 and 0.8 mm, respectively. Liquid N_2 cooled InSb and MCT detectors were used. The frequency resolution was varied from 0.003 to 3 cm^{-1} depending on the bandwidth of the investigated spectral lines. A cutoff filter for the spectral region 2000–3000 cm^{-1} was used to improve the signal/noise ratio.

To investigate cryocrystals in the whole spectral region (from far infrared to ultraviolet) at the *same* sample without changing window material a special sample cell with diamond windows (accessible spectral range 10–43000 cm^{-1}) was designed (Fig. 2). This cell consists of a brass corpus A and two copper discs B with polycrystalline diamond windows C (∅3 mm). The diamond windows are glued onto the coppers discs. The coppers discs are separated by a brass ring D (inner diameter of 10 mm) as a spacer to vary sample thickness. The inner area E between the two coppers discs serves as the sample chamber. The copper was selected as a material for sample chamber to exclude considerable thermal gradient across our sample. The thickness of the samples was 1.2 mm in the present studies. The indium rings were used to seal the sample chamber (shown by dark dots in Fig. 2). A steel capillary tube F connects the sample chamber with the gas system.

The sample cell was mounted on a cold finger of a closed cycled He cryostat (position G in Fig. 2).

The sample temperature was measured by a calibrated Si-diode with a temperature resolution of 0.005 K in the temperature region below 25 K and 0.05 K at higher temperatures. The accuracy of the temperature stabilized by a computer was better than ± 0.01 K at $T \leq 25$ K and ± 0.03 K at higher temperatures. To obtain information on the real absolute sample temperature the Si-diode was calibrated by comparing a registered sample temperature to known fixed thermodynamic temperature points (solid–solid phase transitions, melting and boiling points of 5 substances: H_2 , Ne, CH_4 , O_2 , N_2). This procedure allows us to reach an absolute accuracy of the sample temperature determination about 0.1 K in the whole temperature range from 10 to 120 K.

To ensure good thermal contact with copper discs (position *B* in Fig. 2) a sample gas was condensed in liquid at overpressure of about one bar. This overpressure was being maintained up to a crystal was completely grown. The samples were slowly grown from the liquid to obtain perfect crystals with good optical quality. This crystal quality was immediately controlled by eye (microscope) during growth as well as by the determination of the bandwidth of the MI molecule fundamental at low temperature. The grown crystals were completely transparent to visible light and had very small residual inhomogeneous broadening (about 0.01 cm^{-1}). We could not detect any traces of the IR-inactive N_2 or O_2 vibron (host crystal); consequently, our crystals are perfect. To overcome the difficulties connected with the big volume jump at the γ–β phase transition in solid oxygen (about 5.4% [2]) and to obtain high quality crystals of low temperature O_2-phases a special procedure worked out by [3] was used and slightly modified for our demands. The γ-O_2 crystal of perfect quality was slowly (0.05 K/h) cooled through the γ–β phase transition. At a temperature slightly lower than the γ–β transition point (ΔT = 0.02–0.03 K) a perfect crystal of β-oxygen was grown at constant temperature (temperature fluctuations were smaller than ± 0.02 K). The changes in our samples during whole growth procedure were monitored continuously spectroscopically. During the recrystallization of the β-phase, we observed an increase of the optical transparency of our samples. If the transparency did not improve further more, the crystal of β-oxygen was slowly (0.1 K/min) cooled down. Near phase transitions, the samples were cooled (or warmed) at much slower rate (0.005 K/min). Two series experiments with different admixture/matrix (A/M) ratio were carried out for both matrix materials (N_2 or O_2). In the first series (A), we monitored the behavior of the IR-active molecules, which were present in our sample gases (O_2 , 99.998% and N_2, 99.999%) as residual contaminations: CO_2 in nitrogen (135 ppb) as well as CO (about 40 ppb) and CO_2 (about 1 ppm) in oxygen. In the second series (B), we investigated nitrogen enriched by CO_2 (75 ppm) and oxygen enriched by the CO (about 0.9 ppm).

The methods to determine the impurity concentration in solid nitrogen were described in [1]. In case of the oxygen samples, we determined the A/M ratio via known absorption coefficients [1,4] as well as via partial pressure.

3. Results and discussion

3.1. Investigation of phase transitions

a) **N_2 matrix**. To test our approach – to probe host crystal quality — we first studied the well investigated α–β phase transition in solid nitrogen. This phase transition is a first order phase transition accompanying by a volume jump (about 0.8%) at the equilibrium vapor pressure [5]. The low temperature α-phase of solid N_2 has $Pa3$ cubic structure and possesses long-range orientational order. The hexagonal β-phase (space group $P6_3/mmm$) is an orientationally disordered phase.

To probe indirectly the α–β-phase transition of the matrix (N_2) we monitored the behavior of the CO and CO_2 fundamentals as a function of temperature. Although both substances react sensitively to this phase transition (see [1]), the most obvious changes are observed in the spectroscopic characteristics of the ν_3-CO_2 fundamental (Fig. 3). These changes were completely reproducible at cooling and warming. One ν_3-CO_2 band in the α-phase is split into two bands in the β-phase exactly at the phase transition point (Fig. 3,*a*). The clear jump is observed in the temperature-dependent bandwidth of the MI molecules at this temperature too. These observations, gained by the spectroscopy of MI molecules, are confirmed by monitoring the two-vibron band of α-N_2, which disappears in the β-phase (see [1, Fig. 6]). The integrated intensity of the ν_3-CO_2 fundamental is proportional to the total number of MI CO_2 molecules. The intensity of the one ν_3-CO_2 band in the α-phase is equal to the total intensity of two ν_3-CO_2 bands in the β-N_2 (Fig. 3,*b*). Since the number of MI molecules is constant at this transition, the MI CO_2 molecules must be distributed between two different sites in the β-N_2 , according to two possible orientational positions in the hcp structure of β-N_2 [1].

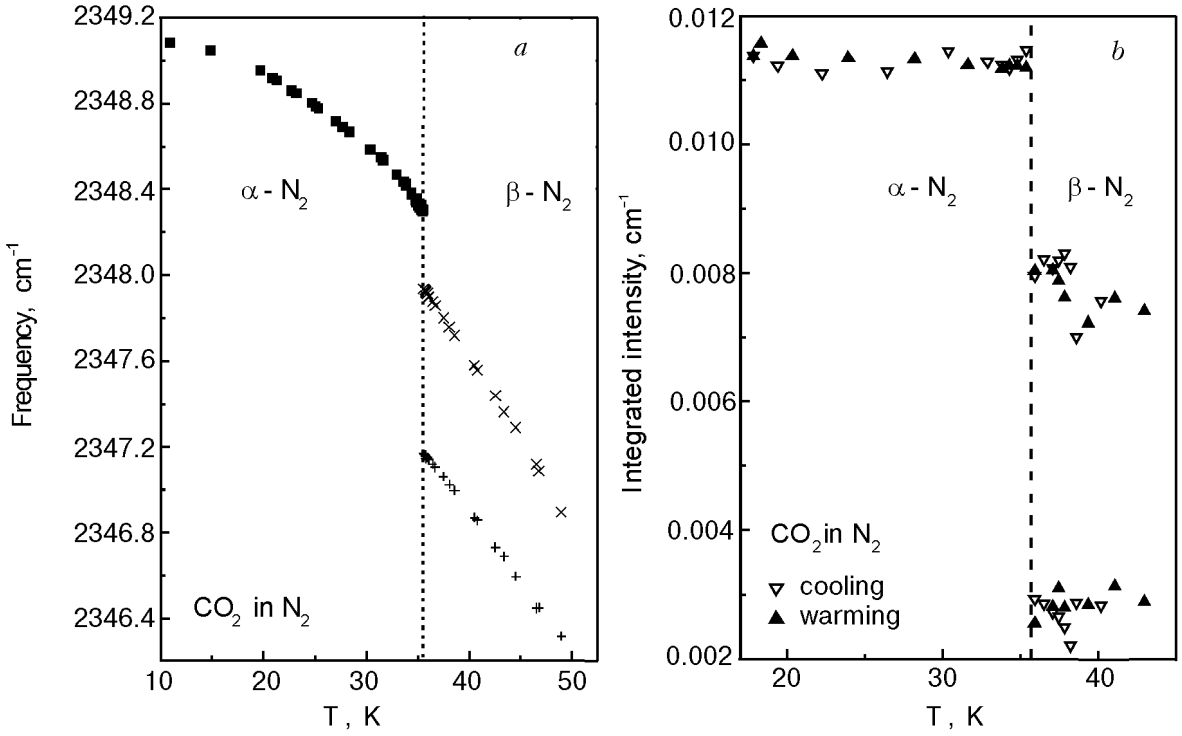

Fig. 3. Temperature dependences of the spectroscopic characteristics of the ν_3-fundamental of CO_2 matrix isolated in solid nitrogen: frequency (*a*) and integrated intensity (*b*). The CO_2 molecules were present in our nitrogen gas (99.999%) as a residual contamination ($CO_2/N_2 = 1.35 \cdot 10^{-7}$).

The detailed analysis of the α–β phase transition [1] showed that the spectroscopic behavior of the CO_2 fundamental mirrors all characteristics of a first order phase transition: a frequency jump; a thermal hysteresis of all of spectroscopic characteristics; the coexistence of the α- and β-phases.

b) **O_2 matrix**. Since 30 years, it is unclear in literature if the α–β phase transition in solid oxygen is of first or second order. We applied the matrix isolation technique to clarify this question.

O_2 molecules possess nonzero electronic spin in the ground electronic state. Therefore, solid oxygen combines properties of a cryocrystal and of a magnetic material. Solid oxygen exists in three phases at ambient pressure: γ-O_2 (T = 54.36–43.8 K), β-O_2 (T = 43.8–23.87 K) and α-O_2 ($T \le$ 23.87 K). The low temperature α-phase is an antiferromagnet [6], whereas the β- and γ-phases possess no long-range magnetic order [7]. The β-O_2 has the rhombohedral lattice of space group $R\bar{3}m$, whereas the structure of the α-O_2 belongs to the space group $C2/m$ [6,8]. The crystal structures of the α- and β-phases are actually very similar and both structures consist of closed-packed layers (basal planes). The distance between nearest molecules in the basal plane (3.2–3.4 Å) is substantially smaller than the distance between nearest neighbors from different layers (≥ 4.2 Å) [2].

The properties of solid oxygen near its phase transitions were extensively investigated by different experimental techniques: by x-ray and neutron diffraction [2,12,14], heat capacity measurements [10,13], IR and Raman spectroscopy [9,22], thermal conductivity [31], etc. However, available either experimental or theoretical data on the order of the α–β phase transition are contradictory. From experimental point of view, the α–β phase transition is considered to be of second order corresponding to the temperature dependence of the magnon frequency observed by [9] and to a λ-like anomaly of the heat capacity observed by [10]. The parallel and perpendicular magnetic susceptibilities do not coincide at the α–β phase transition point [11]. The thermal hysteresis was observed by elastic neutron diffraction [12] and heat capacity measurements [13]. Consequently, we consider this α–β phase transition to be first order based on experimental results by [11–13]. X-ray studies [14] demonstrate that both phases coexist within 1 K near α–β phase transition; however, these authors did not detect any hysteresis.

In theoretical oriented literature [15–17,32], there is also no consensus on the physical origin and classification of the α–β phase transition: pure crystallographic transition, magnetically driven and/or magneto-elastically driven. Different theoretical models to describe this phase transition were ex-

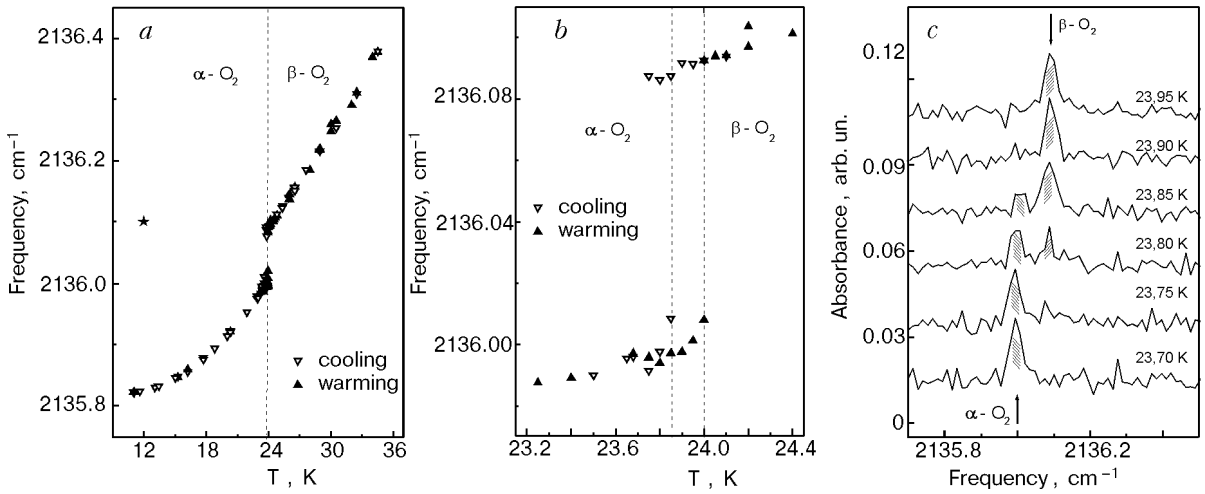

Fig. 4. Temperature behavior of the internal vibration of the CO molecules matrix isolated in solid oxygen ($CO/O_2 \sim 4 \cdot 10^{-8}$): temperature dependence of the CO fundamental frequency (star is the data by [19]) (*a*); thermal hysteresis of the α–β phase transition in solid oxygen (*b*); the coexistence region of the α- and β-phases during cooling by monitoring the CO fundamental band in both phases (*c*). Resolution was 0.003 to 0.037 cm^{-1} and error in absolute frequencies is less than symbol.

ploited to characterize the order of this phase transition. E.g., the authors [15] described the α–β phase transition as a second order transition; according to [17,25], the α–β phase transition is of first order.

To obtain unambiguous experimental information on the order of the α–β phase transition we carefully monitored the behavior of the spectroscopic characteristics of the internal vibration of CO molecules MI in solid oxygen. Due to literature, we found one spectroscopic study on CO dissolved in solid oxygen (resolution 0.25–0.30 cm^{-1}) [18]. CO molecules were produced by UV photolysis of O_2: H_2CO and O_2: $H_2C_2O_2$ (2000:1) solid mixtures at T = 12 K.

Figure 4,*a* shows the temperature dependence of the CO fundamental in α- and β-phases of solid oxygen, reproducible in cooling and warming. At temperatures higher 34 K, the CO peak becomes very broad (bandwidth about 0.1 cm^{-1} at 34 K) and, therefore, cannot be observed at such small CO concentrations. A jump in frequency is clearly visible at the α–β phase transition. This change in the environmental shift of the vibration frequency of the MI molecules ($\omega_{crystal}$–ω_{gas}) is determined by changes (i) in the intermolecular distances of the host crystal as well as by changes (ii) in the host crystal orientational order parameter [1,19].

Figure 4,*b* presents the temperature dependence in fine steps (0.05 K) of the CO fundamental frequency in the vicinity of the α–β phase transition for one of our samples. The temperature, at which the new band shows up as a proof for the new phase, lies at 23.85 and 24 K at cooling and warming, respectively. The concrete temperature values varied from one sample to the other, but these fluctuations were not more than 0.1 K. Our temperature range for hysteresis is a bit smaller than the thermal hysteresis observed by [13].

Figure 4,*c* shows our spectra near the $\beta \rightarrow \alpha$ phase transition. The coexistence region of the α- and β-phases is clearly visible at 23.85 and 23.80 K. This coexistence of the α- and β-phase was observed in every sample (5 series) as well as during cooling and warming.

The jump in the CO fundamental frequency (0.09 ± 0.01 cm^{-1}) at the α–β phase transition is comparable with the temperature-caused changes in frequency in the temperature range of the α-O_2 (0.17 cm^{-1}). Since the intermolecular interaction between O_2 molecules in the basal plane is substantially stronger than the interlayer interaction [20] the jump in the CO frequency is mainly determined by changes in the basal plane. Our own analysis of the structural data by others [2] showed that no discontinuity is observed in the area of the basal plane of a unit cell (presenting the β-phase by monoclinic axes) at the α–β phase transition. Therefore, the frequency shift of 0.09 cm^{-1} obtained by us reflects the monoclinic distortion of the basal plane of solid oxygen, which appears/disappears at the point of the α–β phase transition, and, consequently, can serve like a quantitative measure of this distortion.

Thus, we obtained the strong experimental evidences (frequency jump, thermal hysteresis, coexistence of the α- and β-phases) that the α–β phase

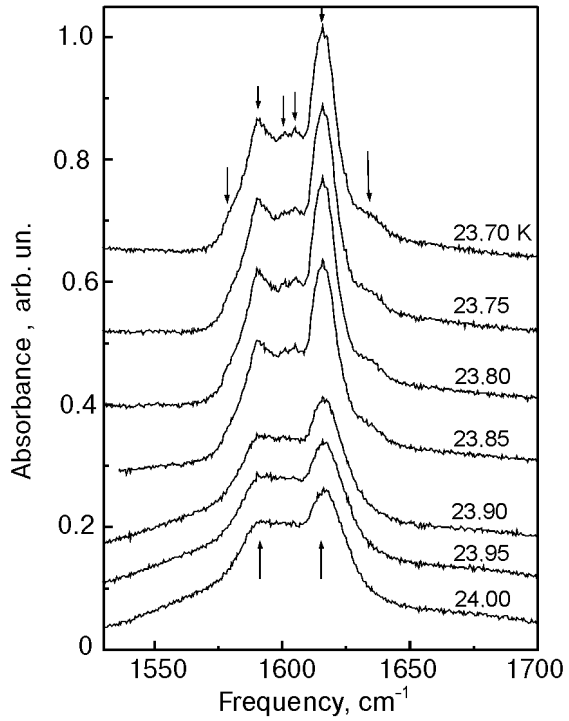

Fig. 5. Spectra of the oxygen vibron side band in the vicinity of the α–β phase transition. The arrows indicate the maxima in the side bands.

transition in solid O_2 is a *first order* phase transition.

This result gained by the analysis of the spectroscopic data of MI molecules, i.e., indirectly, was confirmed by the careful investigation of the behavior of the oxygen vibron side band, i.e., directly. Figure 5 demonstrates the temperature evolution of the side band spectrum in the vicinity of the α–β phase transition by warming the sample. The β-O_2 side band contains only two maxima (at 1591 and 1617 cm^{-1}) without any additional fine structure (spectrum at $T = 24$ K). These maxima were already observed [21] and assigned to an IR absorption of a combination of oxygen vibron ($\nu_0 = 1552$ cm^{-1} [22]) with a libron (39 cm^{-1}) and a lattice phonon (65 cm^{-1}), respectively. Both features exist in the side band of α-oxygen too (spectrum at $T = 23.70$ K). However, the maximum at higher frequency is substantially reinforced in comparison to the one in the β-O_2 side band; the additional contribution originates from the second libron branch (≈ 70 cm^{-1}) existing in α-oxygen only. The α-O_2 side band possesses also an additional fine structure (at frequencies about 1601 and 1606 cm^{-1}) between the two main maxima and two small maxima (at 1580 and 1636 cm^{-1}). The maxima of the fine structure correspond to a combination of the oxygen vibron with lattice phonons at the Brillouin zone boundary — frequencies of 49 and 54 cm^{-1} relatively to the vibron frequency. The features at 1580 and 1636 cm^{-1} relate to a high frequency magnon (frequency about 28 cm^{-1}) and a lattice phonon (frequency about 84 cm^{-1}), respectively. Each of these six values in the phonon sideband spectra for α-O_2 agrees quite well with experimental [9,22] and theoretical [23] data. As it can be seen, no observable changes in spectra occur in the temperature range from 23.7 to 23.85 K. At the temperature 23.9 K, all extra features of the α-O_2 side band are already absent and a typical side band of the β-O_2 is present only. The following increase to 24 K causes no further changes in the spectra. Therefore, the first order phase transition occurs between 23.85 and 23.90 K during warming of the sample. A similar behavior shows up between 23.80 and 23.75 K during cooling of this sample. By other words, a thermal hysteresis takes place in the spectroscopic characteristics of solid oxygen at the α–β phase transition too. It is important to note that these temperature points (23.85 K → 23.90 K and 23.80 K → 23.75 K) coincide exactly with the values determined by monitoring the behavior of the CO molecules in the same sample.

This eminent behavior — such as discontinuity and hysteresis — at the α–β phase transition is not only observed at the vibron side band and at the internal vibration of CO MI in solid oxygen, but also clearly confirmed by us at other elementary excitations of O_2 such as excitons, exciton-vibrons, two-vibron bound states. A two-phase coexistence temperature region was observed too*.

All these spectroscopic results allow us to draw two conclusions: first, the α–β phase transition in solid oxygen is of the first order; second, the changes in the host crystal lattice at a phase transi-

* The coexistence of α- and β-phases near to the α–β phase transition could be caused, in principle, by small temperature gradients in our samples. One may consider several origins for such gradient: 1) heating of our sample by light irradiation; since the illumination of our sample as well as its absorption is different in different regions (mid IR to visible spectral region) and since the two-phase region in our spectra is always present, this is no explanation; 2) a permanent temperature gradient through out the sample due to a cold finger and cell geometry. Since we varied the diaphragms of illumination (from 0.8 to 1.5 mm) and since the spectra also were not affected this cannot be the case. In addition, we studied 5 samples and 11 heating/cooling cycles and reproduced all our results. Therefore, we are convinced to monitor the true phase coexistence region in our spectra.

tion can be successfully probed by the spectroscopy on the guest molecules.

3.2 Indirect estimation of volume changes in the host crystal

In general, the temperature dependence of one mode frequency must contain somehow the temperature dependence of the crystal volume. Therefore, we will try to exploit this to the MI case and deduce information on matrix volume.

An environmental frequency shift of the internal vibration of a MI molecule ($\omega_{crystal}$–ω_{gas}) is determined by the interaction between the embedded molecule and host crystal ones, averaged over relative translational and orientational motions of the impurity and the matrix molecules [19]. The general formulae for the environmental frequency shift of the linear molecules are given in [1]. In our case of CO in solid oxygen and nitrogen (two atomic linear molecules MI in the orientational ordered phases), these expressions can be written in the self-consistent approximation in the following form:

$$\Delta\omega \equiv \omega_{crystal} - \omega_{gas} = \frac{B_e}{\omega_e}\left\{ \sum_j A(R_j) + \eta_{imp} \times \right.$$

$$\left. \times \left[\sum_j U_1(R_j) + \sum_j U_0(R_j)\, \eta_j \right] \right\} = K\, W(R, T) \ . \quad (1)$$

Here B_e and ω_e are the rotational and harmonic vibrational constants of the MI molecule, respectively; η_{imp} and η_j are the orientational order parameter of the MI and host crystal molecules, respectively; R_j is the intermolecular distance between a MI molecule and jth matrix particle; $A(R)$, $U_1(R)$ and $U_0(R)$ are combinations of the first and the second order derivatives of the potential energy of the MI molecule in a matrix with respect to an impurity interatomic distance, which are calculated at equilibrium interatomic distance; $K = B_e/\omega_e$; W is the normalized matrix shift.

Three force constants presented in (1) have different origins: A(R) is determined by the isotropic part of the intermolecular interaction between the MI and host crystal molecules, whereas $U_1(R)$ and $U_0(R)$ are formed by the noncentral part. The force constants A, U_1 , and U_0 in the equation (1) are functions of the distance R between the MI molecule and host crystal molecules. Of course, the host crystal ones is deformed by the impurity around it. The deformation field around an impurity causes some changes in the force constant quantities in comparison to the nondeformed crystal. However, the temperature-caused changes in the deformation field (e.g., an excess volume caused by one impurity) are mainly determined by the thermal expansion of the host crystal [24]. Therefore, we expect that the temperature behavior of the mode frequency of our MI molecule is mainly governed by the thermal expansion of the host crystal lattice too.

We confirmed these general considerations by spectroscopic data for CO molecules MI in α-nitrogen and β-oxygen (Fig. 6,*a*,*b*) (as well as for the CO_2 in solid nitrogen [1]) as follows. Taking in account that the temperature-caused changes in the intermolecular distance of the host crystal are relatively small (about 1%) at the equilibrium vapor

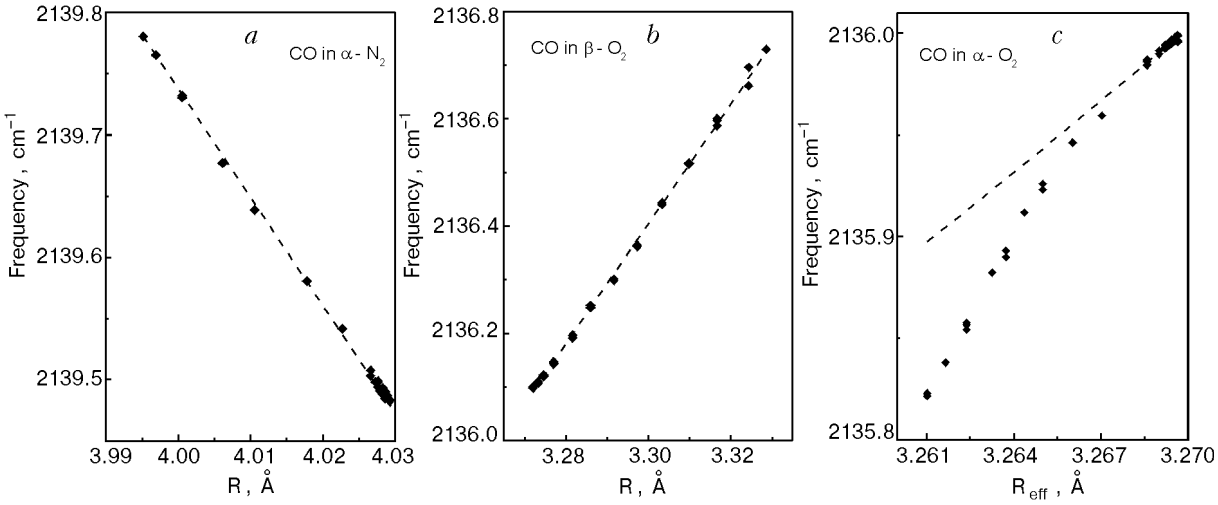

Fig. 6. Internal vibration frequency ω of the CO molecules matrix isolated in orientationally ordered phases of solid nitrogen and oxygen vs. the nearest neighbor separation R: CO in α-nitrogen ($CO/N_2 = 5 \cdot 10^{-7}$) (*a*); CO in β- and α-oxygen (*b*) and (*c*), respectively ($CO/O_2 \sim 4 \cdot 10^{-8}$ as well as $4 \cdot 10^{-7}$). The experimental and theoretical values due to Eq. (1) are shown by diamonds and dashed lines.

pressure, we can expand the normalized matrix shift W in equation (1) into a Taylor series:

$$W(R(T)) = W(R)|_{R_0} + (\partial W/\partial R)|_{R_0} [R(T) - R_0] + \text{higher orders}, \quad (2)$$

R is the distance between nearest neighbors in the α-nitrogen and β-oxygen. Combining Eq. (2) and Eq. (1), we obtain a simple expression to model the experimentally determined mode frequency behavior $\Delta\omega(T)$ in the phases where this behavior is governed by one crystal lattice parameter. The $W(R_0)$ and $\partial W/\partial R_0$ values obtained by modeling the experimental data are presented in Table 1. The nearest neighbor distance R at 0 K and 24 K were chosen as R_0 for the α-N_2 and β-O_2, respectively.

Table 1

Normalized matrix shift of CO fundamental frequency in different matrices *

Host crystal	$W(R_0)$, cm^{-1}	$\partial W/\partial R_0$, cm$^{-1}\cdot$Å^{-1}
α-nitrogen	−3911 ± 11	−9942 ± 412
α- and β-oxygen	−8066 ± 44	−12560 ± 81

* For details, see Eq. (2)

The agreement achieved between experiment and model is excellent (Fig. 6,*a*,*b*). Consequently, it means that spectroscopic data of MI molecules can be successfully used to deduce and estimate the molar volume changes in a host crystal if this is not known!

We drew this conclusion from spectroscopic measurements at equilibrium vapor pressure. Nevertheless, we expect that the same situation takes also place at high pressure qualitatively, i.e., the temperature behavior of the mode frequency of MI molecules during any isobaric route mainly reflects the thermal expansion of the matrix material. To prove our assumption directly, corresponding experiments are planned. Now we would like to discuss this mode frequency behavior of MI molecules in more detail. Comparing Figs. 6,*a* and 6,*b* this behavior of mode frequency of CO molecules MI in solid nitrogen is quite different from the behavior in solid oxygen. This qualitatively different behavior comes from the difference in the nature of the stability of the α-nitrogen and oxygen phases as well as from the difference in the intermolecular potential between the MI molecules and host crystal particles. The α-N_2 structure is stabilized by the *central* part of the intermolecular potential together with the quadrupole component of the noncentral interaction [5], whereas the *noncentral* part of the repulsive interaction is responsible for the stability of the orientational ordered phases of solid oxygen [20]. Therefore, the matrix shift of the fundamentals of impurity molecules is governed by a sum of an isotropic and a quadrupole–quadrupole interaction in case of the α-nitrogen and by the noncentral part of the repulsive interaction in the α- and β-O_2.

An unexpected behavior of the CO fundamental was observed in α-oxygen. We tried to model the experimental frequency $\omega(T)$ or $\omega(R)$ similarly to the situation in β-O_2. Because of the monoclinic distortion in α-oxygen, two independent variables must be used in that case. We chose the effective distance between neighbors R_{eff} ($R_{\text{eff}} = \sqrt{3^{-1/2}S}$, S is the area of the basal plane of a unit cell) and the relative distortion in the b-direction δ ($\delta = b - R_{\text{eff}}$, b is the unit cell parameter). This selected geometry allows us to preserve the similarity of α- and β-phases: R_{eff} shows no discontinuity at the α–β phase transition as S, and δ is zero in β-O_2 by definition. Then, we can paraphrase (2) in a form, which is applicable to the special case of α-O_2:

$$W_{\alpha\text{-}O_2}(R(T), \delta(T)) = W(R_0) + (\partial W/\partial R_0) \times [R_{\text{eff}}(T) - R_0] + (\partial W/\partial\delta)|_o \, \delta(T). \quad (3)$$

As values for $W(R_0)$ and $\partial W/\partial R_0$ in case of α-phase we preserved the corresponding values of β-phase, obtained earlier. The value $(\partial W/\partial\delta)|_0$ was obtained by modeling the experimental dependence at temperatures near the α–β phase transition and is equal to (486 ± 2) cm$^{-1}\cdot$Å^{-1}. This value is substantially smaller than the $\partial W/\partial R_0$ value (see Table 1). It means that the changes in frequency of the CO fundamental in α-oxygen are mainly determined by the changes in the area of the unit cell basal plane S. This result of our modeling is shown by a dashed line in Fig. 6,*c*. The relatively small but distinct discrepancy is seen between the modeled $\omega(R)$ and experimental $\omega(T)$ values. This difference between experiment and theory (about 0.07 cm^{-1}) exceeds considerably the experimental inaccuracy (± 0.005 cm^{-1}). We associate this deviation (Fig. 6,*c*) with an increase in the magnetic order as the temperature decreases. Due to the strong dependence of the exchange interaction J_{ij} on the mutual orientation Ω_{ij} of interacting i and j molecules [23] ($J_{ij} = f(R_{ij}, \Omega_{ij})$), an influence of the magnetic order on the orientational order parameter [26] must be considered here too, i.e., an

increase in the magnetic order causes a mutual increase in the orientational order parameter. Therefore, the difference between the modeled $\omega(R)$, (broken line) and experimental $\omega(T)$ (symbols in Fig. 6,*c*) values reflects the temperature-caused changes in the orientational order parameter, caused by changes in the magnetic order of the α-oxygen, what was not taken in account in Eq. (3).

3.3. Determination of part of the binary phase diagram

a) *Solubility limit of* CO_2 *in oxygen and nitrogen*. In liquid oxygen, we observed the ν_3-fundamental of the CO_2 molecules MI in liquid oxygen at 2342 cm^{-1} (Fig. 7). In our IR spectra of liquid oxygen, we could not observe and identify any other impurity absorptions. This ν_3-CO_2 band is present in the spectra of both series of our samples (*A* and *B*) without substantial differences in frequency, bandwidth and integrated intensity. Therefore, we believe that our oxygen gas contains CO_2 molecules as a residual contamination without external leakage of the vacuum system. We did not find any information in literature about CO_2 molecules in condensed phases of oxygen.

The temperature dependence of the mode frequency and the bandwidth is presented in Fig. 8,*a* and 8,*b* respectively. The spectral resolution was 0.3–3 cm^{-1} at these measurements. Both temperature dependences were quite reproducible at cooling and warming. The profile of the ν_3-CO_2 fundamental is rather well described by a Lorentz function. The temperature dependence of the integrated intensity appeared very surprising for us (Fig. 8,*c*). This behavior was reproducible but not identical at cooling and warming. At cooling, the intensity

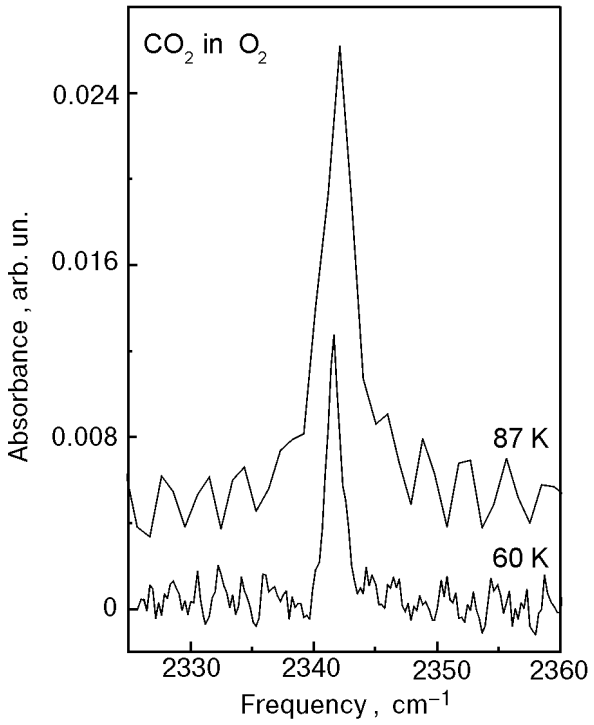

Fig. 7. Spectra of the ν_3-fundamental of the CO_2 molecules matrix isolated in liquid oxygen at two different temperatures. The CO_2 molecules are present in our oxygen (99.998%) as a residual contamination.

increases slightly from 87 to 82 K, remains almost constant to 72 K and decreases rapidly to 60 K. A very weak trace is visible at 57 K and disappears completely near the melting point; no traces of this band are observable in the solid state. This band of the MI CO_2 reappears during warming at 75 K. As the temperature increases, the integrated intensity of this band increases too.

To estimate the amount of CO_2 molecules in liquid oxygen we compared the integrated intensity

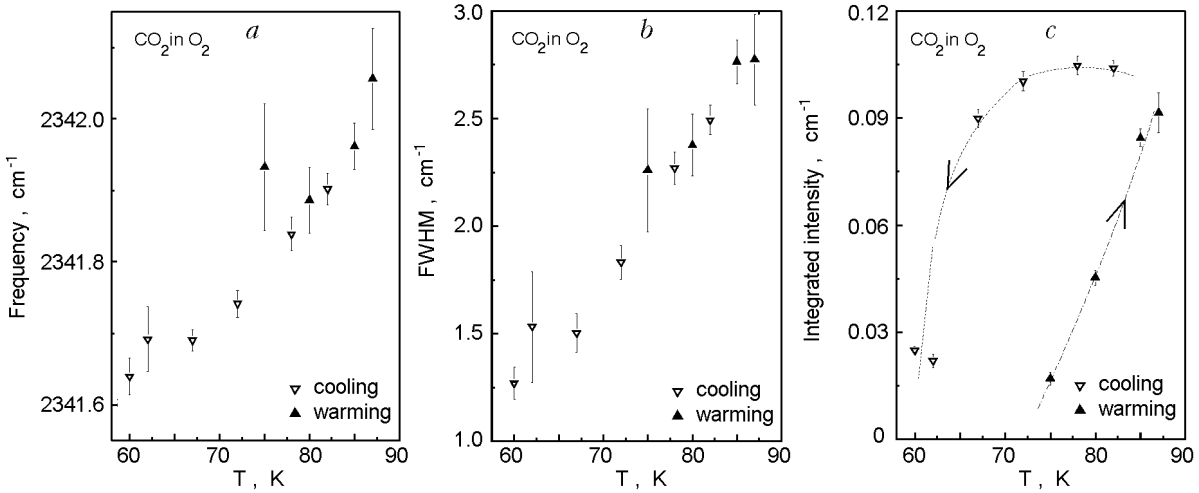

Fig. 8. Temperature dependences of the frequency (*a*), bandwidth (*b*), and integrated intensity (*c*) of the ν_3-internal vibrations of the CO_2 molecules matrix isolated in liquid oxygen (the lines in Fig. 8,*c* emphasis a sequence in time). Bars show experimental inaccuracy.

of the ν_3-CO_2 band in liquid oxygen with our data on the intensity of this band in α-nitrogen (see Fig. 3,*b*). In the latter case, the CO_2 concentration (135 ppb) was independently determined by mass spectroscopy. This comparison shows that the concentration of the CO_2 in liquid oxygen is varied from about 1.4 ppm at 82 K to about 0.19 ppm at 60 K.

We interpret this specific result as a direct determination of the thermodynamic solubility limit of CO_2 in oxygen. The solubility of the CO_2 in liquid oxygen reduces as the temperature decreases and becomes practically zero in solid oxygen: the CO_2 molecules evaporate out of the sample. During warming of the sample, CO_2 molecules are again dissolved in the sample. The different behavior at opposite temperature routes can originate from differences in kinetics during evaporation and dissolution.

A similar small solubility is also observed for the CO_2 in solid nitrogen [1]. In nitrogen samples doped with 75 ppm CO_2 (series *B*), we observed spectroscopically crystalline clusters of about 200 CO_2 molecules in solid N_2. Besides this band due to clusters an additional band was observed, which we assigned to the ν_3-mode of CO_2 molecules matrix isolated in N_2. Due to Ref. 1, we believe that the solubility limit of the CO_2 in solid nitrogen lies at about (or less) 1 ppm.

b) *Influence of small amount of* CO *on phase transitions in solid oxygen.* No information on O_2–-CO phase diagram exists up to now [27]. To investigate part of the O_2-CO phase diagram at small concentrations of CO we premixed 0.9 ppm CO gas with O_2 gas (series *B* of our samples), condensed this gas mixture at 87 K and grew the crystal samples as it was described in Sec. 2. Only monomers of CO were observed in these samples. The integrated intensity of the CO band is 0.008 ± 0.001 cm^{-1}. Using the absolute absorption coefficient for gaseous CO [4], we estimate the actual concentration of the CO in solid oxygen ($3–4 \cdot 10^{-7}$). The temperature evolution of the CO fundamental band near the α–β phase transition during cooling is shown in Fig. 9,*a*. One can clearly recognize that the intensity of the CO band in β-O_2 is decreasing, whereas the intensity in α-O_2 is increasing as temperature decreases. Therefore, we can associate these changes in spectra (Fig. 9,*a*) to the changes in the phase composition of the sample during the α–β phase transition. This transition is extended for 0.6 K (23.90–23.30 K in Fig. 9,*a*) in this series of our samples in comparison to 0.15 K in samples of series *A* (Fig. 4,*c*). In general, two external factors control a phase transformation rate at first order phase transition: (i) degree of overcooling (or overheating), i.e., the difference between the actual temperature and temperature of the transition point (23.90 K in the case shown in

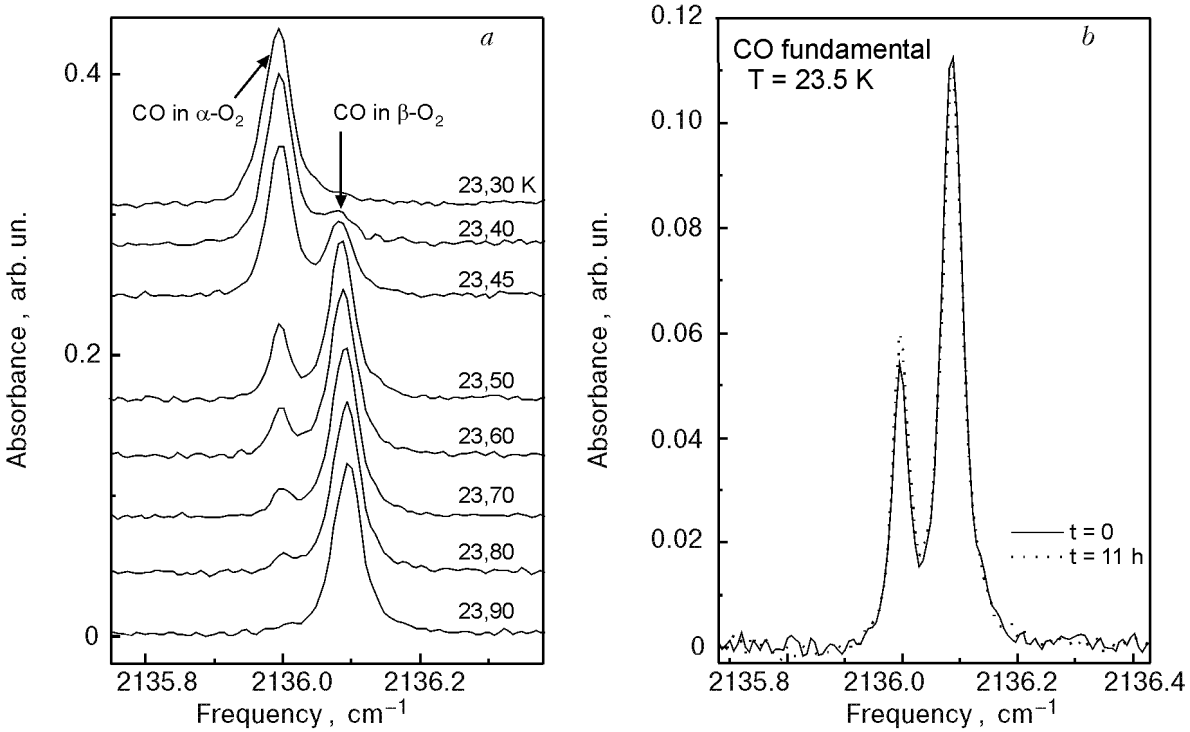

Fig. 9. Spectra of the CO band in the coexistence region of the α- and β-phases of solid oxygen ($CO/O_2 \sim 4 \cdot 10^{-7}$) during cooling: temperature evolution (*a*); spectra recorded at 23.5 K just after a temperature decreased (solid line) and 11 h later (dashed line) (*b*). Resolution is 0.015 cm^{-1}.

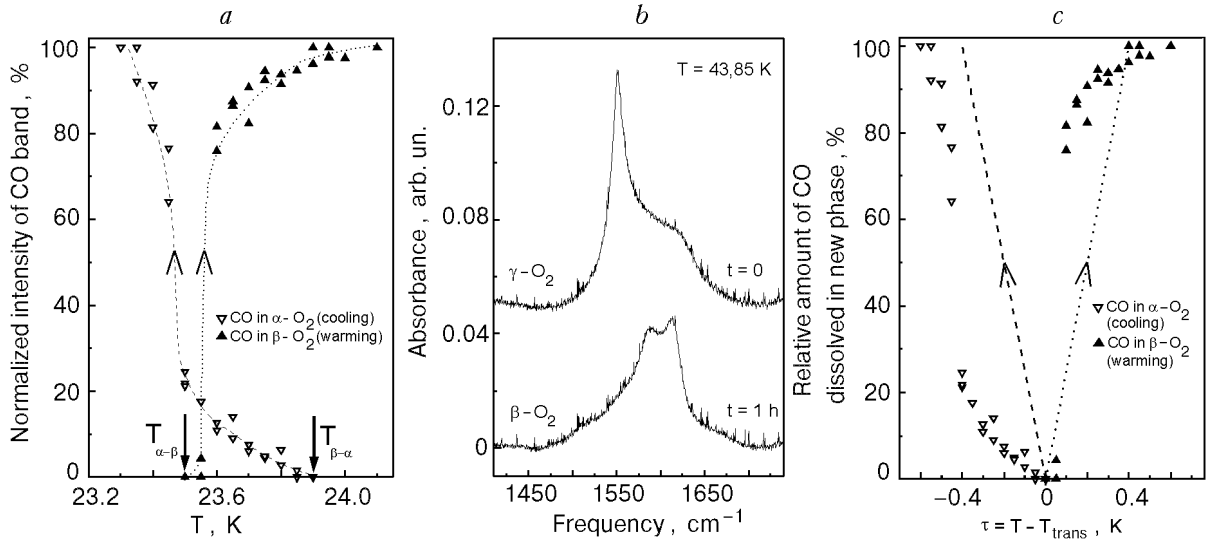

Fig. 10. Influence of CO molecules (concentration $\sim 4 \cdot 10^{-7}$) on phase transitions in solid oxygen: the ratio of the integrated intensity of the CO band in α-phase during cooling (∇) and in β-phase during warming (▲) to the total intensity of two coexisting phases (*a*); the vibron side bands recorded during $\gamma \to \beta$ phase transition just after a temperature decreased (γ-phase) and 1 hour later (β-phase) (*b*); the same experimental values as in Fig. 10,*a* in comparison to the portion of CO molecules dissolved in the new phase calculated by Eq. 4 using Gibbs phase rule (dashed lines — at cooling, dotted line — at warming) as a function of a suitable relative temperature $\tau = T - T_{trans}$ (*c*).

Fig. 9,*a*) and (ii) exposure time at concrete temperature point in two-phase temperature region. To determine which factor mainly rules the kinetics of the α–β phase transition in solid oxygen, some spectra were specially recorded during this phase transition at constant temperature as a function of time up to hours. About 3% of new phase were created during 11 h at the constant temperature only, as displayed in Fig. 9,*b*. The following decrease in temperature of 0.05 K creates about 40% of new phase (the time of recording of spectrum is about 3 h) (see Fig. 9,*a*). Therefore, time-depending kinetics does not play a significant role at the α–β phase transition in solid oxygen unlike the α–β phase transition in solid nitrogen (see [1, Fig. 7,*c*]).

To investigate the influence of CO on the α–β phase transition more detailed, we monitored the behavior of the CO fundamental near this transition in both opposite temperature routes (during cooling and warming) and determined the integrated intensity of the CO bands in both coexisting phases. The ratio of the integrated intensity of the CO band in α-phase (at $\beta \to \alpha$ phase transition) and in β-phase (at $\alpha \to \beta$ phase transition) to the total intensity of two coexisting bands corresponds to the relative portion of CO molecules dissolved in this phase C_{imp} ($0 \le C_{imp} \le 1$) (Fig. 10,*a*). It is obvious that the transition at warming ($T_{\alpha \to \beta}$) begins at lower temperature than the transition at cooling ($T_{\beta \to \alpha}$), i.e., the α–β transition in solid oxygen has been split in two transitions in these samples!

According to our considerations, there are two reasons for this feature ($T_{\alpha \to \beta} < T_{\beta \to \alpha}$). First, this temperature behavior results from some peculiarities of the α–β phase transition (magnetic + structural transitions, intermediate phase, etc.) and due to relatively high intensity of the CO band in these samples, this special oxygen feature could be observed. Second, it is a usual splitting of phase transitions in binary systems (O_2–CO in our case). To differentiate between these two possibilities we probed the β–γ phase transition by monitoring the oxygen vibron side band, whose shape is qualitatively different in these two phases (see Fig. 10,*b*). Temperature steps of 0.05 K were used. A shift of about 0.2 K towards higher temperatures is clearly observed for our samples enriched by CO (see Table 2).

Table 2

The β–γ phase transition points obtained monitoring the vibron sidebands

Samples	Temperature of the phase transition, K	
	$\gamma \to \beta$ (at cooling)	$\beta \to \gamma$ (at warming)
A (O_2 , 99,998%)	43,65	43,90
B (O_2 + 0,9 ppm CO)	43,85	44,00

It means that CO molecules influence indeed the phase transitions in solid oxygen even at such small concentrations (about $4 \cdot 10^{-7}$)!

The second remarkable feature in Fig. 10,*a* is the different temperature behavior of the integrated intensity of CO bands during $\beta \to \alpha$ and $\alpha \to \beta$ phase transitions. In general, the phase transformation in two-phase region is accompanied by two processes: first, a changing in volume ratio of coexisting phases and second, a changing in the concentration of the impurity in these phases. Both processes influence the temperature dependence of the C_{imp} values. Therefore, the difference in kinetics of $\beta \to \alpha$ and $\alpha \to \beta$ phase transitions, observed by monitoring the intensity of CO bands, could result, in principle, from the thermodynamic equilibrium redistribution of the CO molecules between two coexisting phases. To verify this explanation of the results observed, we calculated the relative amount of the impurity dissolved in a new phase (C_{imp}) in two-phase temperature region using the Gibbs phase rule. Due to very small concentrations of a second component, we presumed that both phase boundaries are linear functions of a total impurity concentration. As a result, we obtained the following simple equation for the temperature dependence of the C_{imp} values:

$$C_{\text{imp}} = |\tau| / (T^{c}_{\text{trans}} - T^{w}_{\text{trans}}) , \quad \tau = T - T_{\text{trans}} . \quad (4)$$

Here T^{c}_{trans} and T^{w}_{trans} are the transition points at cooling and warming, respectively ($T_{\beta \to \alpha}$ and $T_{\alpha \to \beta}$ in our case); T_{trans} is a transition point at a thermal route that is considered; $T_{\alpha \to \beta} \le T \le T_{\beta \to \alpha}$; $0 \le C_{\text{imp}} \le 1$.

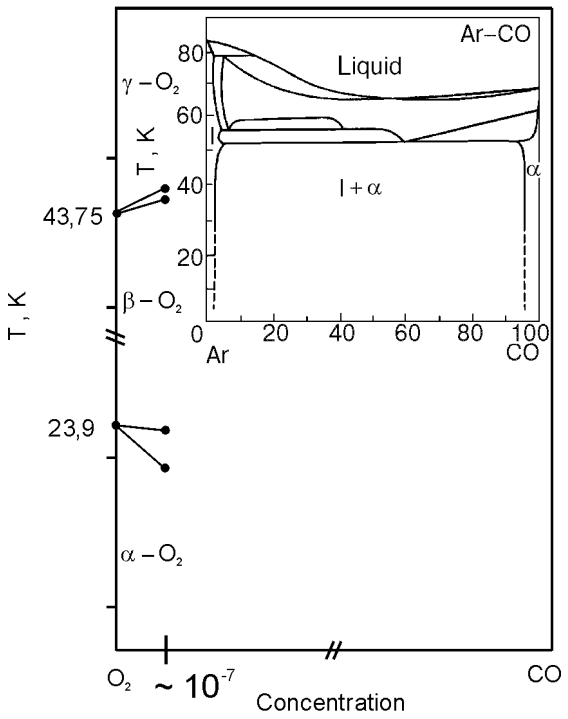

Fig. 11. Oxygen-rich part of O_2–CO phase diagram. The Ar–CO diagram [27] is used for illustration purposes.

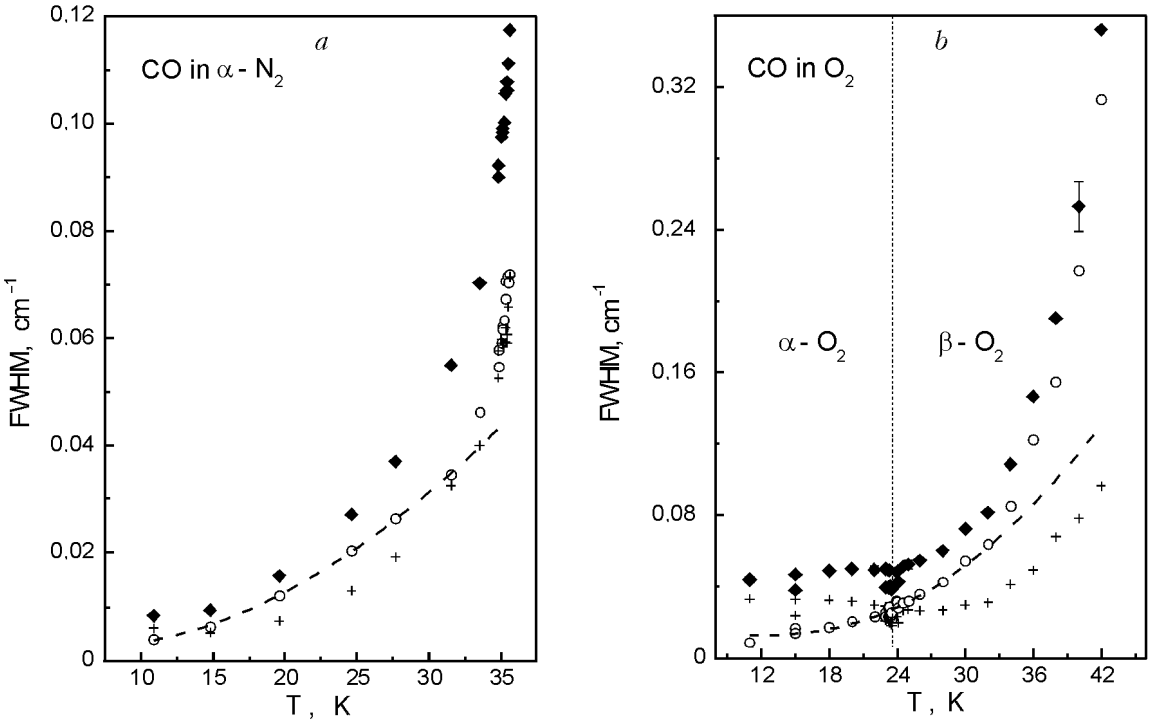

Fig. 12. Temperature dependences of the CO fundamental bandwidth in the orientationally ordered phases of solid nitrogen (*a*) and oxygen (*b*) (experimental values, ◆): the spectral profile of this band was first deconvoluted into a Lorentzian (○) and a Gaussian (+) band. The dashed line shows our fit of the bandwidth by pure Lorentzian bandshape.

According to the thermodynamic calculations (Eq. (4)), the temperature-caused changes in C_{imp} must be identical during cooling and warming. However, this is not the case (Fig. 10,*c*). By decreasing temperature, the experimental C_{imp} values increase noticeably slower than the calculated ones at $\tau \geq -0.4$ K. At $\tau = -0.45$ K ($T = 23.45$ K), the relative portion of CO molecules dissolved in α-phase increases practically by jump and shows behavior similar to the theory by following lowering temperature. At the $\alpha \rightarrow \beta$ phase transition (warming), the portion of new β-phase growths very quickly at $\tau = 0.1$ K ($T = 23.6$ K) and changes very slowly at higher temperatures. All these changes were *completely* reproducible during every temperature cycle. According to our opinion, two different physical mechanisms are responsible for these peculiarities of the kinetics of the α–β phase transition. First, the nucleation and the growth of the new phase inside β- and α-phases create different deformation fields and, therefore, elastic strains accompanying the $\alpha \rightarrow \beta$ transition are different during opposite temperature routes. Second, nonmagnetic β-phase is nucleated on the CO impurities; therefore, CO molecules accelerate the $\alpha \rightarrow \beta$ phase transition.

The O_2-rich part of O_2–CO phase diagram reconstructed from our results is shown in Fig. 11. We expect peritectoid and eutectoid points for the β–γ and α–β phase transitions, respectively, at higher concentrations of CO. Remarkably, our diagram starts at concentration as low as $\sim 10^{-7}$ whereas usual $T - x\%$ diagrams start at % only (see phase diagram as inset in Fig. 11).

3.4. Bandwidth of the CO fundamental in solid nitrogen and oxygen

For possible theoretical studies, we display the temperature dependences of CO mode in O_2 in Table 3. Figure 12 shows the temperature dependence of the CO fundamental bandwidth in solid nitrogen and solid oxygen for comparison. The temperature dependence of FWHM of the fundamental band of the CO molecules MI in solid oxygen does not show any noticeable changes at the α–β phase transition. To model the measured profile of absorption bands of MI CO molecules a Voigt function was used. Then this Voigt profile was deconvoluted into a Gaussian and Lorentzian component as shown in Fig. 12.

a) **Gaussian bandwidth**. In general [1], the Gaussian bandwidth is a superposition of an inhomogeneous broadening and a quasistatic broadening. The former results from some host crystal imperfections and has practically no temperature dependence. The latter originates from instantaneous fluctuations of the environmental frequency shift of the impurity internal vibration because of orientational and translational motions of both dissolved and host crystal molecules. That is why the quasistatic broadening possesses a temperature dependence. Both components of the Gaussian bandwidth contribute to the residual ($T \rightarrow 0$ K) Gaussian broadening; however, only the inhomogeneous broadening can serve as a measure to characterize crystal structure perfection.

Table 3

Frequencies of the CO fundamental in orientationally ordered phases of solid oxygen (experimental inaccuracy ±0.005 cm^{-1})

Temperature, K	ω_{0-1}, cm^{-1}
α-oxygen	
11	2135,822
13	2135,838
15	2135,855
17	2135,882
18	2135,891
19	2135,912
20	2135,924
21	2135,946
22	2135,959
23	2135,986
23.5	2135,999
β-oxygen	
24	2136,099
24.5	2136,108
25	2136,121
26	2136,144
28	2136,193
30	2136,249
32	2136,299
34	2136,363
36	2136,442
38	2136,517
40	2136,594
42	2136,672

The Gaussian component of the CO fundamental bandwidth in solid nitrogen is characterized by small values at low temperature (Fig. 12,*a*). Corresponding to our modeling [1], the inhomogeneous broadening is zero in that case and the residual Gaussian broadening ($T \to 0$ K) is determined by the zero-point oscillations of the CO and N_2 molecules.

The Gaussian bandwidth of the CO fundamental in solid oxygen is much larger in comparison to case of solid N_2 and has no clear temperature dependence at low temperatures. Therefore, the residual Gaussian broadening of the CO band ($T \to 0$ K) is mainly determined by imperfections of the oxygen crystal.

The Gaussian component of the fundamental bandwidth of CO in N_2 and in O_2 is characterized by a pronounced temperature dependence at temperatures higher than 20 and 30 K (Fig. 12), due to quasistatic broadening. Near phase transitions, fluctuations of orientational order become very large and cause therefore a strong increase in the Gaussian bandwidth (e.g., about 5 K below $T_{\alpha\beta}$ in solid nitrogen).

b) **Lorentzian bandwidth**. The Lorentzian bandwidth broadening of the impurity fundamental is determined by depopulation and dephasing processes and can be modeled by the following formula at not too high temperatures:

$$\Delta_L = B_{\text{depop}}(1 + n_{\text{depop}}) + B_{\text{deph}}\, n_{\text{deph}}(1 + n_{\text{deph}}) \,. \quad (5)$$

Here B_{depop}, n_{depop} and B_{deph}, n_{deph} are the squares of the effective anharmonic coupling coefficients and the occupation numbers of corresponding phonons (ω_{depop} and ω_{deph}) for the depopulation and dephasing processes, respectively [28].

The dephasing process, in Eq. (5) may contain two physically different kinds of the lowest order quartic processes: a dephasing by host crystal lattice phonons [28] and a dephasing by localized (or quasi-localized) modes induced by an impurity [29]. Now we model the experimental temperature dependence of the Lorentzian bandwidth by Eq. (5). First step: in case of CO molecules MI in both crystals, only one depopulation decay channel exists at low temperatures, i.e., energy transfer to the isotope ^{13}CO. That is why we chose the difference between the frequencies of ^{12}CO and ^{13}CO isotopes (47.2 cm^{-1}) as a frequency ω_{depop} of lattice phonons involved in the depopulation processes. Because ω_{depop} is about 50 cm^{-1} and the concentration of the ^{13}CO isotope is very low, the contribution of depopulation processes to the Lorentzian bandwidth is expected to be very small. Second step: we varied three other parameters (B_{depop}, B_{deph}, and ω_{deph}) in Eq. (5). The result of our modeling is shown in Figs. 12,*a* and 12,*b* by dashed lines. The frequencies of phonons involved as well as the values of anharmonic coefficients obtained by modeling are presented in Table 4. In case of α-nitrogen the frequency ω_{deph} (31 cm^{-1}) of a mode suited for a dephasing process matches very well with the frequency of one of the maxima of the phonon density of states (DOS) of the host crystal [5]. It means that the coupling of the CO internal vibrations with the α-N_2 lattice phonons is responsible for the broadening of the CO fundamental by dephasing processes. The vibronic dephasing of the CO molecules MI in solid oxygen is governed by a mode with frequency $\omega_{\text{deph}} = 77$ cm^{-1} (Table 4). This frequency is close to the high frequency boundary of the phonon density of states of solid oxygen (83 cm^{-1}) and does not match with its maxima (40 and 70 cm^{-1}) [30]. We think that this mode at $\omega_{\text{deph}} = 77$ cm^{-1} corresponds to a localized mode generated by perturbations embedding CO molecules in the oxygen crystal. This analysis shows that the CO molecules fit into a nitrogen crystal whereas the CO molecules cause significant perturbations in the oxygen crystal.

Table 4

Parameters of the relaxation processes determining Lorentzian broadening of the CO bandwidth in α-nitrogen and orientationally ordered phases of solid oxygen

Matrix	ω_{depop}	B_{depop}	ωdeph	B_{deph}
	cm^{-1}			
α-nitrogen	47,2	0.003	31	0.08
Oxygen	47,2	0.013	77	1.5

Our modeling of the Lorentzian broadening of the CO fundamental gives reasonable results only up to 32 K for both matrices. The pure dephasing mechanism results from the anharmonic interaction between the MI and host crystal molecules. Because we considered only lowest order quartic processes in Eq. (5), the observed discrepancy between experimental values and fitted values shows that higher terms of dephasing processes must be taken into account at higher temperatures.

4. Conclusion

Our aim was twofold: first, to realize the *real* matrix isolated case (impurity/matrix ratio $\sim 10^{-7}$–10^{-8}); second, to probe the matrix material by analyzing the data of the matrix isolated molecules. This was achieved for CO and CO_2 isolated in solid nitrogen and oxygen by FTIR spectroscopy. We investigated several impurity concentrations, we were able to grow optically perfect crystals (inhomogeneous bandwidth), cooling and heating the sample over a wide range proofed reproducibility of measurements.

From our spectroscopic data we are able to draw conclusions about the matrix isolated particle and its coupling to the matrix: from mid IR spectra we determined the frequency, bandwidth, integrated intensity, bandshape of the molecule vibration (CO and CO_2) as a function of temperature, concentration and matrix (O_2 and N_2). For example: the measured bandshape (Voigt profile) was modeled by a Gaussian and Lorentzian component. The Gaussian part of the bandwidth contains two terms: the inhomogeneous term mirrors crystal quality ($\Gamma(T \to 0) < 0.01$ cm^{-1}) and the quasistatic term is related to the orientational and translational relative motions between impurity and matrix molecules. Near phase transitions, this quasistatic contribution to the Gaussian bandwidth increases enormously and we characterize this anomalous behavior as a precursor to the phase transition. The Lorentzian part of the bandwidth is mainly governed by dephasing processes via lattice phonons (including localized modes) and hardly ruled by depopulation processes via isotopes of impurity molecules.

From our spectroscopic data of matrix-isolated molecule, we are able to draw conclusions indirectly about the matrix itself. We are able to classify the order of phase transitions of the matrix material via fingerprints in spectra (jump in frequency, hysteresis, coexistence of phases, etc.). This method was confirmed by direct observation of phonon side bands and two-vibron band of matrix, which show a distinct behavior at phase transitions. From the temperature dependence of the environmental frequency shift ($\omega_{crystal} - \omega_{gas}$) of impurity vibrations, we could unambiguously draw conclusions about the thermal expansion of the matrix material, sometimes not known. Commonly, the matrix-isolated case is realized by 1‰ or 1%, whereas we studied an impurity/matrix ratio of about 10^{-7}–10^{-8}. Therefore, we could make correct statements about the influence of the amount of impurities on the phase transition of the matrix and clearly determine solubility limits (CO_2 in N_2 or O_2 about 1 ppm).

Acknowledgment

This work was supported by Deutsche Forschungsgemeinschaft (grant No. Jo 86/11-1) and H. J. J acknowledges support by the NATO (grant No. 950285). We appreciate the help of S. Medvedev during the last stages of experiments. The authors are grateful to both referees for critical remarks.

1. M. Vetter, M. Jordan, A. P. Brodyanski, and H. J. Jodl, *J. Phys. Chem.* **A104**, 3698, (2000).
2. I. N. Krupskii, A. I. Prokhvatilov, Yu. A. Freiman, and A. I. Erenburg, *Sov. J. Low Temp. Phys.* **5**, 130 (1979).
3. A. F. Prikhotko, Yu. G. Pikus, and L. I. Shanskii, *Opt. Spectros. (USSR)* **54**, 277 (1983).
4. P. Varasani and S. Sarangi, *J. Quant. Spectry. Radiat. Transfer* **15**, 473 (1975); B. Schurin and R.E. Ellis, *J. Chem. Phys.* **45**, 2528, (1966); C. L. Korb, R. H. Hunt, and E. K. Plyler, *J. Chem. Phys.* **48**, 4252 (1968).
5. *Physics of cryocrystals*, V. G. Manzhelii, and Yu. A. Freiman (eds.), AIP, Woodbury, New York (1997).
6. R. A. Alikhanov, *JETP Lett.* **5**, 430 (1967); R. J. Meier and R. B. Helmholdt, Phys. Rev. B29, 1387 (1984).
7. M. F. Collins, *Proc. Phys. Soc.* **89**, 415 (1966); D. E. Cox, E. J. Samuelssen, and K. H. Beckurts, *Phys. Rev.* **B7**, 3102 (1973); F. Leoni and F. Sacchetti, *Phys. Rev.* **B7**, 3112 (1973).
8. C. S. Barret, L. Meyer, and J. Wasserman, *J. Chem. Phys.* **47**, 592 (1967).
9. T. G. Blocker, M. A. Kinch, and F. G. West, *Phys. Rev. Lett.* **22**, 853 (1969).
10. C. H. Fagerstroem and A. C. Hollis-Hallet, *J. Low Temp. Phys.* **1**, 3 (1969).
11. C. Uyeda, K. Sugiyama, and M. Date, *J. Phys. Soc. Jpn.* **54**, 1107 (1985).
12. P. W. Stephens and C. F. Majkrzak, *Phys. Rev.* **B33**, 1 (1986).
13. L. Lipinski, A. Szmirka-Grzebyk, and H. Manuszkiewicz, *Cryogenics* **36**, 921 (1996); *J. Low Temp. Phys.* **111**, 399 (1998).
14. A. S. Baryl'nik and A. I. Prokhvatilov, *Low Temp. Phys.* **20**, 716 (1994).
15. V. A. Slyusarev, Yu. A. Freiman, and R. P. Yankelevich, *JETP Lett.* **30**, 270 (1979); *Sov. J. Low Temp. Phys.* **6**, 105 (1980); *ibid.* **7**, 265 (1981).
16. Yu. B. Gaididei and V. M. Loktev, *Sov. J. Low Temp. Phys.* **7**, 643 (1981).
17. B. Kuchta, T. Luty, and R. J. Meier, *J. Phys. C: Solid State Phys.* **20**, 585 (1987).
18. M. Diem, Tai-Ly Tso, and E. K. C. Lee, *Chem. Phys.* **73**, 283 (1982).
19. A. D. Buckingham, *Faraday Soc. Trans.* **56**, 26 (1960).
20. A. P. Brodyanskii and Yu. A. Freiman, *Sov. J. Low Temp. Phys.* **11**, 231 (1985).
21. H. W. Lowen, K. D. Bier, and H. J. Jodl, *J. Chem. Phys.* **93**, 8565 (1990).
22. K. D. Bier and H. J. Jodl, *J. Chem. Phys.* **81**, 1192 (1984).
23. A. P. J. Jansen and A. van der Avoird, *J. Chem. Phys.* **86**, 3583 (1987).

24. L. D. Yantsevich, *Ph. D. thesis*, Institute for Low Temperature Physics and Engineering, Kharkov, (1987); A. P. Brodyanskii and M. A. Strzhemechny, *Sov. J. Low Temp. Phys.* **16**, 203 (1990); M. A. Strzhemechny, A. I. Prokhvatilov, and L. D. Yantsevich, *Physica* **B198**, 267 (1994).
25. A. J. R. da Silva and L. M. Falicov, *Phys. Rev.* **B52**, 2325 (1995).
26. A. P. Brodyanskii and Yu. A. Freiman, *Sov. J. Low Temp. Phys.* **11**, 548 (1985).
27. V. G. Manzhelii, A. I. Prokhvatilov, I. Ya. Minchina, and L. D. Yantsevich, *Handbook of Binary Solutions of Cryocrystals*, Begel house, New York (1996).
28. P. Foggi and V. Schettino, *Rivista del nuovo cimento* **15**, 1 (1992).
29. D. J. Diestler and A. H. Zewail, *J. Chem. Phys.* **71**, 3103 (1979); *ibid.* **71**, 3113 (1979); D. Robert and L. Galatry, *ibid.* **64**, 2721 (1976).
30. R. D. Etters, K. Kobashi, and J. Belak, *Phys. Rev.* **B32**, 4097 (1985).
31. A. Jezowski, P. Stachowiak, V. V. Sumarokov, J. Mucha, and Yu. A. Freiman, *Phys. Rev. Lett.* **71**, 97 (1993).
32. J. M. Dundon, *Phys. Lett.* **61A**, 58 (1977); E. Domany and E. K. Riedel, *Phys. Rev. Lett.* **40**, 561 (1978).